https://doi.org/10.5194/egusphere-2026-2474
Preprint. Discussion started: 6 July 2026
© Author(s) 2026. CC BY 4.0 License.

A Numerical Weather Prediction Model-Based Approach to Assess Fire Weather Conditions over the Northwest Himalayan Forests

Anandu Prabhakaran[1], Piyush Srivastava[1]

[1]Centre of Excellence in Disaster Mitigation and Management, Indian Institute of Technology Roorkee, Roorkee, Uttarakhand, 247667, India

Correspondence to: Piyush Srivastava (piyush.srivastava@dm.iitr.ac.in)

Abstract

In recent years, forest fire activities have increased in frequency and intensity over the Indian Himalayan region. Year 2024 witnessed numerous fires spread across the Himalayan states of India, causing devastating economic and environmental impacts. The sparse observational network across the Himalayas significantly limits the availability of real-time data, thereby constraining the timely dissemination of wildfire early warnings. This study elaborates on utilising an NWP model, such as the Weather Research and Forecasting Model, for the simulation of fire weather variables for the 2024 summer fire season across the northwestern Himalayan states. A very high-resolution WRF model is configured with the NCEP-FNL reanalysis dataset as the initial and boundary conditions, and simulations are carried out to reconstruct high-resolution fire weather conditions during the 2024 fire weather season across 24 identified fire clusters. The analysis suggests that the two major fire weather indicators (1) Vapour Pressure Deficit and (2) Fire weather indices from the Canadian Fire Danger Rating System blended with NWP model simulations could be a potential tool in identifying fire weather conditions for data sparse complex terrains and subsequently issuing fire weather alerts on a daily basis where the current Fire Danger rating system operates at 10-day intervals.

1. Introduction

Climate change and associated global warming are drivers of more frequent and extended wildfire events globally (Abatzoglou et al., 2025; Bhattarai et al., 2025; Jones et al., 2022; Ruffault et al., 2018). The increase in frequent and intense wildfire events has garnered global attention over the past few decades, with the crucial requirement of early warning systems to minimise the impact of wildfires. Over the past few years, effective wildfire management and mitigation efforts have reduced wildfire-related casualties (Kalogiannidis et al., 2025). However, fire events, including Chile wildfires, California wildfires, Canadian wildfires, and Australian wildfires, have gained global attention, with significant forested land burning and wildfire emissions transported across continents (Hoffman et al., 2022; Jain et al., 2024; Keeley, 2004; Nolan et al., 2020; Turco et al., 2023; Yu et al., 2020). Despite global advancement in fire danger rating systems and wildfire early warning systems, the management of large-scale atmospheric circulation-driven wildfires in the changing climate remains a persistent and complex problem (Carta et al., 2023; Flannigan et al., 2009; Jones et al., 2022).

https://doi.org/10.5194/egusphere-2026-2474
Preprint. Discussion started: 6 July 2026
© Author(s) 2026. CC BY 4.0 License.

The Indian region, located in the tropics, is prone to multiple fire events annually starting from early October to late June, depending on the onset of the southwest monsoon, which brings intense downpours across the country (FSI, 2021, 2023). The geographical extent and varying weather patterns significantly affect the fire season across the country (Mina et al., 2023; Ocón et al., 2021; Prabhakaran & Srivastava, 2024, 2026). Although fires can be natural, the anthropogenic influence on forest fires remains a critical cause for the ignition of fires with the increasing population near the wildland urban interface (WUI) across the Indian region (Mina et al., 2023; Prasad et al., 2008), with the governing factors for the spread of fires depending on the existing meteorological, topographical, geographical and fuel conditions (Holsinger et al., 2016; Zahura et al., 2024). Over the past few decades, the Himalayan foothills have witnessed multiple wildfire events annually, with the northwestern Himalayan states, including Himachal Pradesh and Uttarakhand (India), experiencing numerous large fires. The rise of winter wildfires with the weakening of western disturbances is on the rise, with the antecedent precipitation prior to the fire season governing the spread of fires over this region (Hunt et al., 2019, 2025; Hunt & Zaz, 2023; Prabhakaran & Srivastava, 2024). The geographical location in the foothills of the Himalayas, with fires over this complex mountain terrain, is modulated by the complex topography and valley breeze (Mina et al., 2023; Prabhakaran & Srivastava, 2024).

Since forest fires pose significant environmental and economic concerns in the Indian region, there exists a strong requirement to improve the existing wildfire early warning system for operational forecasting. The current operational Forest Fire Danger Rating System (FFDRS) over the Indian region utilises the Canadian Fire Weather Index (FWI) (Figure S3 & S4) to disseminate the probable fire danger with a lead time of 07 days (Forest Survey of India, 2021). Furthermore, the fires detected by the Moderate Resolution Imaging Spectroradiometer (MODIS) sensor (1000 m x 1000 m spatial resolution) and Suomi National Polar-orbiting Partnership (S-NPP) sensors (375 x 375 m spatial resolution) are disseminated to citizens on a geolocation basis to alert the communities residing in vulnerable locations across the country. Moreover, meteorological datasets from the India Meteorological Department (IMD) are further integrated to provide prefire alerts via the National Disaster Alert portal (SACHET) under the National Disaster Management Authority, Government of India (NDMA, 2021) (Figure S4).

Although wildfires have seen a gradual rise over the Himalayas, complex and undulating Himalayan terrain along with limited accessibility to remote locations results in sparse in-situ meteorological observations. Wildfires over the Himalayan region occur in relatively smaller scale in patches which may be further accelerated by the slope alignment and the corresponding meteorological conditions. This limits the capture of real-time atmospheric conditions and the fire weather feedback generated by the fires across observational networks. There has been an increase in the number of AWS stations in recent years but the lack of long-term (decadal-scale) continuous observational data over the study area poses challenges to analyse the fire-atmosphere interaction processes. Further, in the absence of dense observational networks, the numerical weather prediction (NWP) model offers a physically

https://doi.org/10.5194/egusphere-2026-2474
Preprint. Discussion started: 6 July 2026
© Author(s) 2026. CC BY 4.0 License.

consistent and spatially continuous tool for hindcasting as well as forecasting the fire weather conditions over data-sparse regions (Di Giuseppe et al., 2016, 2020; James et al., 2025; Vitolo et al., 2018). The NWP models simulate meteorological variables, including near-surface temperature, relative humidity, wind speed, precipitation and the essential fire weather parameters, at a higher spatial and temporal resolution compared to the spatially sparse ground-based measurements (Mölders, 2008; Tang et al., 2013). Furthermore, the NWP model outputs may be continuously integrated into operational forest fire early warning systems (FFEWSs), enabling the dissemination of fire weather indices where surface observations are sparse or absent (Tang et al., 2013). Several fire behaviour tools, such as FARSITE (Ager et al., 2011; Finney, 1998) and BehavePlus (Andrews et al., 2005; Andrews & Bevins, 2003), are employed to simulate the spread of fires by integrating fuel, terrain and meteorological parameters within the Rothermel surface fire spread framework. However, they assume steady-state assumptions, which fundamentally breakdown in the complex and rugged Himalayan terrain (Cruz & Alexander, 2013; Finney, 1998; Sullivan, 2009). Moreover, during prolonged fire events under rapidly evolving atmospheric conditions, FARSITE struggles with crown fire dynamics owing to its dependence on empirical parameterisations and simplified combustion physics. Both FARSITE and related tools assume fuel to be spatially continuous and homogeneous within pixels and do not account for fire-atmosphere interactions during fire weather scenarios (Ager et al., 2011; Price & Germino, 2022). BehavePlus is a point-based system where the meteorological and fuel conditions are kept constant for each calculation, which limits the model from predicting the spatiotemporal evolution of fire weather conditions. Similar to FARSITE, BehavePlus utilises average fuel attribute values per pixel without accounting for the spatial variability in the fuel structure (Ager et al., 2011; Andrews & Bevins, 2003). Although global NWP models such as GFS (Global Forecast System, NOAA/NCEP), IFS (Integrated Forecast System, ECMWF) and UKESM (UK Met office Unified Model) are capable of capturing synoptic-scale fire weather patterns, their coarse spatial resolution ($0.^{25°}$ to $^{1°}$) is insufficient to resolve the mesoscale thermodynamic and wind structures that govern the spread of fires in complex mountainous terrain (J. Singh et al., 2021, 2024). The application of a high-resolution regional NWP model represents a reliable alternative for fire weather forecasting over the Himalayas.

The Weather Research and Forecasting (WRF) model has been widely used as a mesoscale forecast model for high-resolution regional weather forecasts across the world (Powers et al., 2017; Skamarock WC, 2008). The WRF model solves the nonhydrostatic compressible equations of motion on a terrain following vertical coordinates, enabling realistic simulation of orographically driven flows, including slope winds, valley breezes, and fire weather environments, which crucially modulate the surface fire weather conditions, resulting in fires creating their own environment (Skamarock WC, 2008). Multiple studies of wildfire events have been conducted across the globe, including the Santa Ana wind event-induced fire spread in California (Jin et al., 2014; Kumar et al., 2023), the foehn-driven

https://doi.org/10.5194/egusphere-2026-2474
Preprint. Discussion started: 6 July 2026
© Author(s) 2026. CC BY 4.0 License.

fire episode (Gohm et al., 2004; Solomos et al., 2018) across the European Alps, and the premonsoon dry spells over the South Asian forests (Mondal & Sukumar, 2014; Prabhakaran & Srivastava, 2024).

This study elaborates on utilising the WRF model as a tool to simulate atmospheric conditions conducive to the spread of fires over the ecologically vulnerable Himalayan states. Furthermore, the model simulations using the local and nonlocal PBL schemes are validated against in situ observational and reanalysis datasets. As the model is validated, the prototype is further evaluated against the prior and postfire scenario variations in meteorological variables, fire weather indices, and vapour pressure deficit, resulting in the progressive spread of fires.

2. Study Area, Data and Methodology

2.1 Study Area

The states of Himachal Pradesh (Geographical Coordinates Latitude 30°22' N to 33°12' N Longitude 75°45' E to 79°04' E & Geographical area 55,673 km^2) and Uttarakhand (Latitude 28°43' N to 31°28' N Longitude 77°34' E to 81°03' E & Geographical area 53,483.36 km^2) located in the foothills of the Himalayas, India (Figure 1) are prone to several fire events annually starting from the early winter season in November to early or late June depending on the arrival of the Southwest monsoon (FSI, 2021, 2023). Both states witnessed significant fires in the year 2024, with the burned area extending over 60000 ha during the 2024 wildfire season. Apart from the forest fire season from March to June, winter wildfires are another scenario that gained attention recently, with immense forested lands burned during the winter duration, where the near-surface temperature was less than 2°C (Mina et al., 2023). Both states possess vegetation rich in Chir pine (*Pinus roxburghii*) and oak (*Quercus leucotrichophora*), with the fire - weather conditions starting from the early winter season extending until the monsoon season (FSI, 2023). The dry weather, along with the accumulated dry fuels in the geographically complex Himalayan region, accelerates the spread of fires post ignition, with the impact of wind speed in the form of valley breeze, solar radiation, lack of moisture and near-surface processes.

https://doi.org/10.5194/egusphere-2026-2474
Preprint. Discussion started: 6 July 2026
© Author(s) 2026. CC BY 4.0 License.

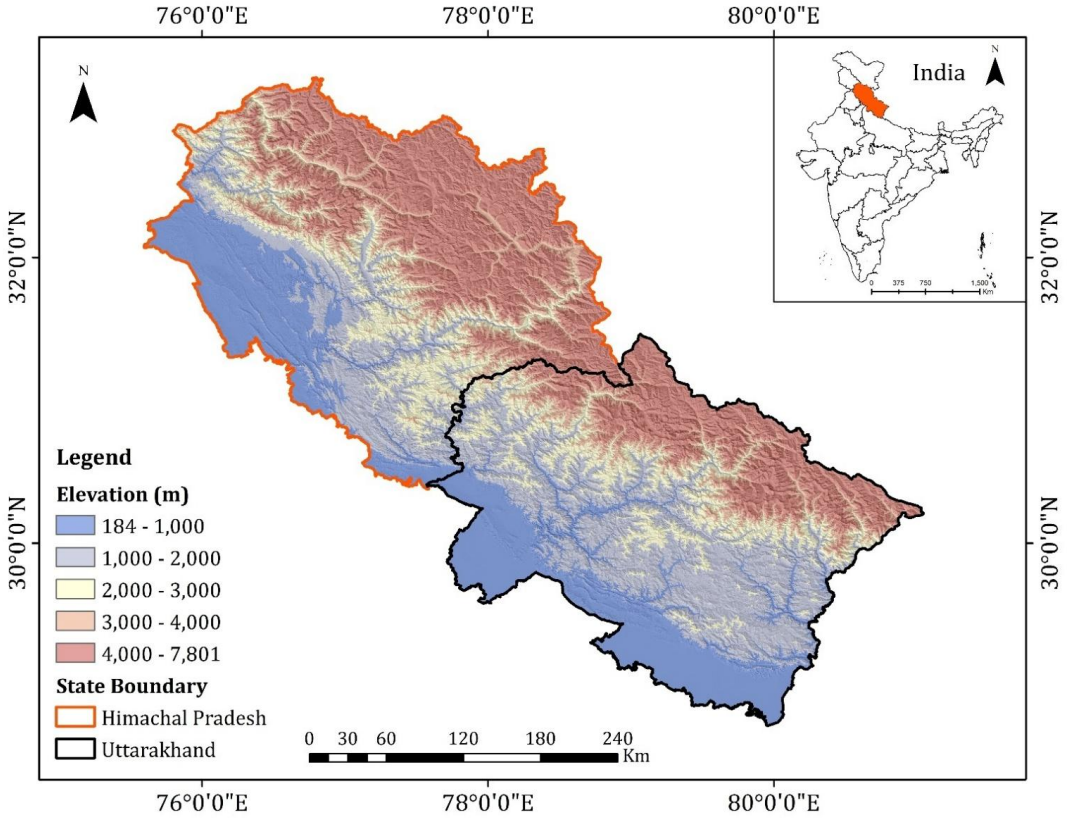

Figure 1 Study area located in the foothills of the Himalayas with Himachal Pradesh (highlighted in red) and Uttarakhand (highlighted in black), India (© Survey of India, downloaded from: https://onlinemaps.surveyofindia.gov.in/Home.aspx, last accessed on 10 February, 2026)).

2.2 Data

A combination of observational and reanalysis datasets is used for the study. The PBL-specific simulations are carried out using the NCEP-FNL dataset (NCEP - FNL, 2000) as the initial and boundary conditions for the WRF model. The in-situ observations from the automated weather stations of the IMD maintained sites across the state of Himachal Pradesh (HP) and Uttarakhand are used to validate the model results. However, the lack of multiple observatories across the study area limits the usage of observational datasets alone. In the absence of observational datasets, a combination of ERA5-Land (Muñoz Sabater, 2019) and ERA5 (H. Hersbach et al., 2020) data may be used as an alternative to evaluate the resulting meteorological conditions (Bhattacharyya et al., 2025) over the Indian region. Furthermore, ERA5 and ERA5-Land data are used to evaluate the relative humidity, wind speed, planetary boundary layer height (PBLH), fire weather indices, vapour pressure deficit (VPD) and sensible heat flux (HFX) arising during fire weather conditions. A summary of the datasets used, along with their spatiotemporal resolution, is summarised in Table 1.

https://doi.org/10.5194/egusphere-2026-2474
Preprint. Discussion started: 6 July 2026
© Author(s) 2026. CC BY 4.0 License.

Sl no.	Meteorological variable	Source	Spatial resolution	Temporal resolution
1.	Initial and Boundary conditions to the WRF model	NCEP-FNL	1° x 1°	06:00 hours
2.	2 m temperature	IMD	Point – based data	hourly
3.	2 m temperature	ERA5 – Land	0.1° x 0.1°	hourly
4.	2 m dew point temperature	ERA5 – Land	0.1° x 0.1°	hourly
5.	Wind speed	ERA5 – Land	0.1° x 0.1°	hourly
6.	Precipitation	ERA5 – Land	0.1° x 0.1°	hourly
7.	Surface sensible heat flux	ERA5 – Land	0.1° x 0.1°	hourly
8.	Boundary Layer Height	ERA5	0.25° x 0.25°	hourly

Table 1 Summary of dataset used for model simulation as well as the in situ observational and reanalysis dataset across the fire clusters.

2.3 Methodology

In this study, WRF version 4.3.3 is configured with an outer domain at 5 km grid spacing, while the nested inner domain preserves a resolution of 1 km (Figure 2), which explicitly resolves the valley winds and other thermodynamic features that are relevant to simulate the meteorological variables conducive to the spread of fires over the Indian Himalayan region during the month of May 2024. The study duration coincided with the excessive heatwave and drought conditions persisting across the North Indian region (India Meteorological Department (IMD), 2024d, 2024c, 2024a, 2024b). Moreover, the summer season of 2024 coincided with the withdrawal phase of a strong El Nino event that affected the weather conditions over the Indian region (Athira et al., 2023; Burton et al., 2020; Prabhakaran & Srivastava, 2026). Although the WRF model is capable of simulating mesoscale features, the accuracy of the simulation depends on the choice of physical parameterisation schemes used to represent the subgrid scale processes that cannot be explicitly resolved at the model grid spacing (Cohen et al., 2015; Powers et al., 2017). The unresolved processes, including turbulent mixing, radiative transfer, land–atmosphere energy exchange, and cloud formation, are represented by means of parameterisation schemes through empirical or semiempirical formulations derived from observational and theoretical understanding (Khairoutdinov et al., 2005; J. Singh et al., 2021; S. Singh & Srivastava, 2025). These formulations allow the model to approximate the aggregate effects of these processes on the resolved atmospheric flow (Cohen et al., 2015). The principal parameterisation modules in the WRF model include the planetary boundary layer (PBL), land surface model (LSM), surface layer, microphysics, cumulus, and radiation schemes (Skamarock WC, 2008). Among these factors, the PBL scheme holds great significance, as the fire weather environment is directly controlled by vertical mixing of heat, momentum and moisture within the atmospheric boundary layer, which further governs the near-surface temperature, humidity, daytime boundary layer growth, wind profile and surface energy balance (Gilliam & Pleim, 2010; Griffin & Otkin, 2022; Kumar et al., 2023). The errors arising from the improper PBL representation thus propagate directly into the fire weather index, which is governed by

https://doi.org/10.5194/egusphere-2026-2474
Preprint. Discussion started: 6 July 2026
© Author(s) 2026. CC BY 4.0 License.

basic meteorological variables, including temperature, relative humidity, precipitation and wind speed (Coen et al., 2013; Mandel et al., 2011; Shin & Hong, 2015).

WRF encompasses a range of PBL parameterisation processes broadly classified into nonlocal first-order closure and local turbulent kinetic energy (TKE)-based closure approaches, where both approaches possess distinct assumptions about vertical mixing mechanisms (Cohen et al., 2015; Mantovani Júnior et al., 2023; Shin & Hong, 2015). For this study, two schemes, YSU (Yonsei University), which is a nonlocal closure scheme, and MYNN (Mellor – Yamada – Nakanishi – Niino), which applies a 1.5-order local closure scheme, are used in combination with the appropriate physical parameterisation schemes. The YSU scheme employs a nonlocal closure where the turbulent diffusivity is determined by a bulk profile shape function and an explicit counter gradient term, which accounts for the heat and moisture transport by the large convective eddies that span over the entire boundary layer depth. This produces well-mixed, deep daytime boundary layers with realistic capping inversions and vigorous entrainment characteristics, which align with observations over heterogeneous and elevated terrains (Hong et al., 2006; Hu et al., 2013; Skamarock WC, 2008; Xie et al., 2012). Meanwhile, the MYNN scheme applies a 1.5-order local closure where the eddy diffusivities are derived from the prognostically computed TKE at each model level, making the mixing responsive to shear and buoyancy but less effective at representing the large plume structures that dominate the convective boundary layer dynamics (Nakanishi & Niino, 2004; Skamarock WC, 2008).

For the study, the simulations were conducted in blocks of 05 days with the first 24 hours excluded to reduce the impact of model initialisation and ensure physically consistent atmospheric evolution. A total of 47 vertical eta levels were incorporated in the simulations to adequately resolve the vertical structure of the atmospheric boundary layer and near-surface processes. Other parameterisation schemes, including longwave and shortwave radiation, surface physics, land surface option, cloud microphysics and cumulus parameterisation, remain the same in both PBL schemes (Table 2).

PBL Scheme	**MYNN**	**YSU**
Longwave	RRTM longwave Radiation	
Shortwave	Dudhia Shortwave Radiation Scheme	
Surface Physics	Revised MM5 Scheme	
Land Surface option	Unified Noah Land Surface Model	
Cloud Microphysics	Purdue Lin Scheme	
Cumulus Parameterisation	Kain-Fritsch Cumulus Scheme (only d01)	

Table 2 This table defines the WRF model setup and corresponding parameterisation schemes used in the simulation.

https://doi.org/10.5194/egusphere-2026-2474
Preprint. Discussion started: 6 July 2026
© Author(s) 2026. CC BY 4.0 License.

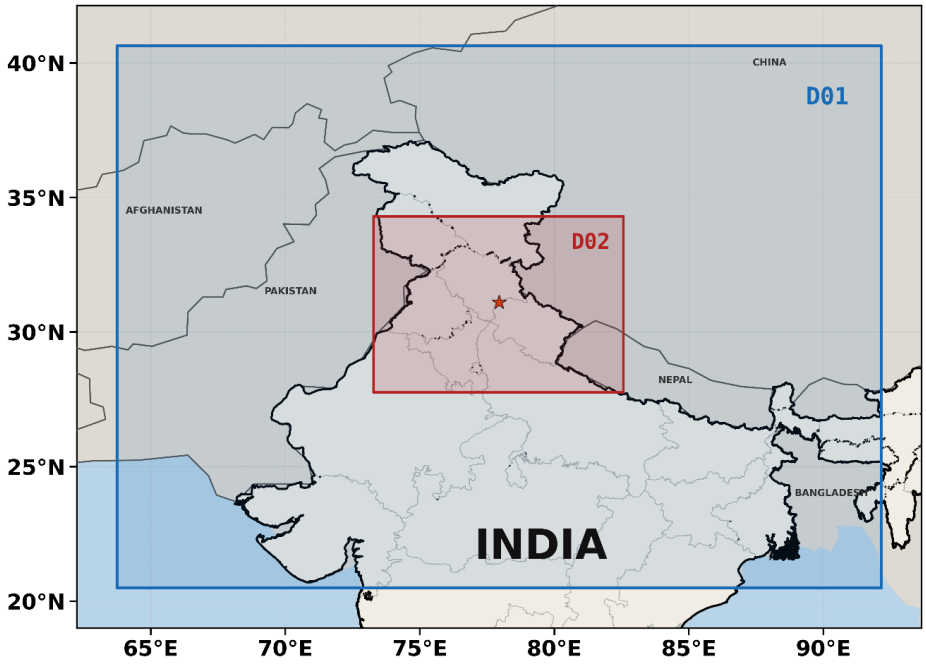

205

Figure 2 This figure shows the study area with the outer domain (D01, 5 x 5 km - blue shade) and nested inner domain (D02, 1 x 1 km – red shade) covering the Northwest Himalayan region (© Survey of India, downloaded from: https://onlinemaps.surveyofindia.gov.in/Home.aspx, last accessed on 10 February, 2026)

https://doi.org/10.5194/egusphere-2026-2474
Preprint. Discussion started: 6 July 2026
© Author(s) 2026. CC BY 4.0 License.

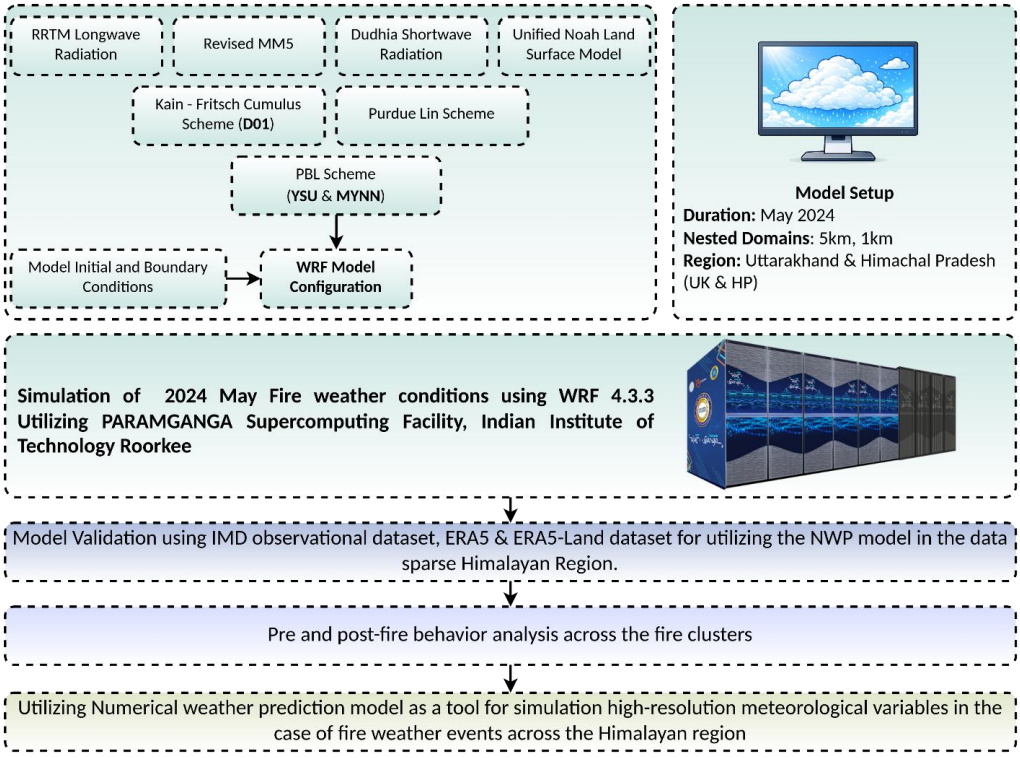

Figure 3 This diagram represents the methodology, including the model setup, numerical simulation and validation.

A combination of an in situ observational dataset from the IMD and a reanalysis dataset from the European Centre for Medium-Range Weather Forecasts is used to validate the modelled results with observations. Furthermore, the fire alerts over the Northwest Himalayan region are filtered out using a high confidence fire interval from both MODIS and S-NPP satellites to deduce the fire events over the Indian Himalayan region. The model simulations are compared with the observational dataset across 98 automated weather stations of the IMD (Figure S1). Furthermore, a total of 16 major fire clusters are identified during the fire window across Uttarakhand and 08 major fire clusters over Himachal Pradesh (Table S1, Figure 4 to Figure 10 & S19 to S24), India. Figure S2 shows the detailed spatial fire distribution map over the states of Himachal Pradesh and Uttarakhand, scattered across the foothills of the Himalayas. The fire clusters are classified on the basis of observable fire alerts obtained over the study domain (Table S1). The inner domain with a 1 km resolution is used for model performance evaluation. The model performance is further evaluated with the ECMWF Reanalysis Version 5 (ERA5) and ERA5-Land data using the Python 3.8 regridding algorithm for model evaluation at the same spatiotemporal reference. Statistical analysis, including correlation coefficient, root mean square error (RMSE), mean bias, and index of agreement, is performed to understand which PBL scheme

https://doi.org/10.5194/egusphere-2026-2474
Preprint. Discussion started: 6 July 2026
© Author(s) 2026. CC BY 4.0 License.

better represents the fire weather conditions. Furthermore, the VPD governing the drying power of the atmosphere was calculated using Teten's equation as follows:

$$VPD = e_s\left(1 - \frac{RH}{100}\right) \quad (1)$$

where

VPD - Vapour pressure deficit (in kPa)

$e_s(T)$ - Saturation vapour pressure at air temperature T (kPa).

RH - Relative humidity (%).

Apart from the basic meteorological variables, the vapour pressure deficit and fire weather index (FWI) from the Canadian fire danger rating system (Lawson & Armitage, 2008) are calculated to further identify the significance of choosing different PBL schemes for fire weather simulation. The fire clusters are used as fire ignition points to evaluate the variations in PBLH, FWI, VPD, and sensible and latent heat fluxes during the fire weather scenario. Moreover, FWI is computed from the daily fire noon (12:00 pm IST) values of relative humidity, temperature, precipitation and wind speed via drought code (DC), duff moisture code (DMC), fine fuel moisture code (FFMC), initial spread index (ISI) and build up index (BUI) following the standard FWI calculation procedure (Lawson & Armitage, 2008). The inputs from the WRF simulations are utilised to generate the FWI over the Himalayan foothills at a 1 km resolution. Since the Canadian FWI values are not standardised with a defined maximum, a fixed upper bound is not defined in the study conducted. For a complete representation of the methodological approach, refer to Figure 3.

3 Results and Discussion

The initial step involves the validation of the meteorological variables simulated using local and nonlocal PBL schemes and characterisation of the associated fire weather environment responsible for the spread of forest fires. The meteorological variables include 2 m temperature, relative humidity, surface sensible heat flux, planetary boundary layer height, and wind speed. Since precipitation remains relatively lower during the pre-monsoon season, the validation of precipitation has been discarded from the following study. Once the applicability of NWP model is established, the fire weather indices and VPD are validated to understand the fire weather characteristics conducive to fire evolution and resulting spread.

3.1 Temperature (2 meters) & Relative Humidity

Forest fires across the states of Himachal Pradesh and Uttarakhand, India, coincide with the summer season from April to June (FSI, 2023). Although winter wildfires are prominent over the study area, summer fires dominate in terms of burned areas and fire intensity (FSI, 2019, 2021). The 2024 wildfire activity over the Indian Himalayan region was dominated by convective boundary layer development (PBLH > 3000 meters) and persistently higher surface temperatures, with the coincidence of heatwave

https://doi.org/10.5194/egusphere-2026-2474
Preprint. Discussion started: 6 July 2026
© Author(s) 2026. CC BY 4.0 License.

conditions existing over the North Indian region (India Meteorological Department (IMD), 2024b, 2024d, 2024c, 2024a). WRF simulations during the fire period are validated against the observational datasets from IMD. The validation of the 2 m temperature against the 98 stations (Figure S5 – S18) across the Himalayan states is summarised in Table 3. Both the YSU_{NCEP} and $MYNN_{NCEP}$ simulations resulted in nearly similar statistical skill scores, with YSU_{NCEP} performing comparatively better than the $MYNN_{NCEP}$ simulations. Over HP, the YSU_{NCEP} simulations generated a mean Pearson correlation of 0.866 and an RMSE of 3.39°C, whereas the $MYNN_{NCEP}$ produced an R value of 0.860 and an RMSE of 3.47°C. However, over Uttarakhand, the YSU_{NCEP} simulation shows a mean R value of 0.844 with a mean RMSE of 3.43, while the $MYNN_{NCEP}$ simulation results in a mean R value of 0.840 and RMSE of 3.5°C. Both states possess a positive bias in 2 m temperature, with YSU_{NCEP} showing +0.64 and +1.32°C and $MYNN_{NCEP}$ showing +0.68°C and +1.41°C over the HP and Uttarakhand, respectively. In the HP, weather stations located at the valley floor sites exhibited positive biases in both schemes, exhibiting bias values exceeding 3.1°C. Across the state of Uttarakhand, nearly 71 of 85 (YSU_{NCEP}) and 72 out of 85 ($MYNN_{NCEP}$) stations show a positive 2 m temperature bias.

Region	Scheme	Mean R	Mean RMSE (°C)	Mean Bias (°C)	N stations
HP	MYNN	0.860	3.47	+0.68	13
HP	YSU	0.866	3.39	+0.64	13
Uttarakhand	MYNN	0.840	3.50	+1.41	85
Uttarakhand	YSU	0.844	3.43	+1.32	85

Table 3 Summary validation statistics for 2 m temperature with an in situ observational dataset from the India Meteorological Department and WRF simulations using the MYNN and YSU–PBL schemes.

The lack of spatially continuous in situ observational networks is further compensated by the ERA5-Land dataset for relative humidity (RH), wind speed, sensible heat flux and planetary boundary layer (Hersbach et al., 2023; Muñoz Sabater, 2019). RH validations across the 16 fire spots derived from the study domain show considerable dry bias across the simulations, with the ERA5-Land reference mean RH ranging from ~32 to 53%, while both simulations exhibit values within 18 to 33%, with YSU_{NCEP} simulations performing marginally better across all metrics (Table 4). However, none of the RH simulations outperformed the ERA5-Land climatological mean as a reference at the fire cluster locations. The dry biases are visible across multiple fire locations with P05 (30.411°N, 78.38°E) and P07 (30.368°N, 78.427°E) on fire dates 28 May 2024, located near the Uttarakhand Himalayas, which exceeded the ERA5-Land reference by 52% with the WRF simulation mean restricted within 20 to 22%, resulting in bias values of -30.50% and -31.56% for $YSU_{NCEP,}$ while the $MYNN_{NCEP}$ simulation biases were -31.48% and -32.49%. When comparing the RH across the fire points, nearly all the fire

https://doi.org/10.5194/egusphere-2026-2474
Preprint. Discussion started: 6 July 2026
© Author(s) 2026. CC BY 4.0 License.

clusters depict spatially consistent RH variation irrespective of the slope aspect, which indicates that synoptic-scale atmospheric forcing dominates over the local topographic microclimate effects in the 2024 Himalayan fires as the fire progresses. However, the south-facing slopes remain consistently drier than the north-facing slopes prior to the fire season (Måren et al., 2015; Schaefer et al., 2024; Yang et al., 2020). Although the bias remains comparatively positive, both simulations could capture the diurnal variations in the resulting RH. Overall, the model performs reasonably well in simulating the near-surface air temperature and relative humidity.

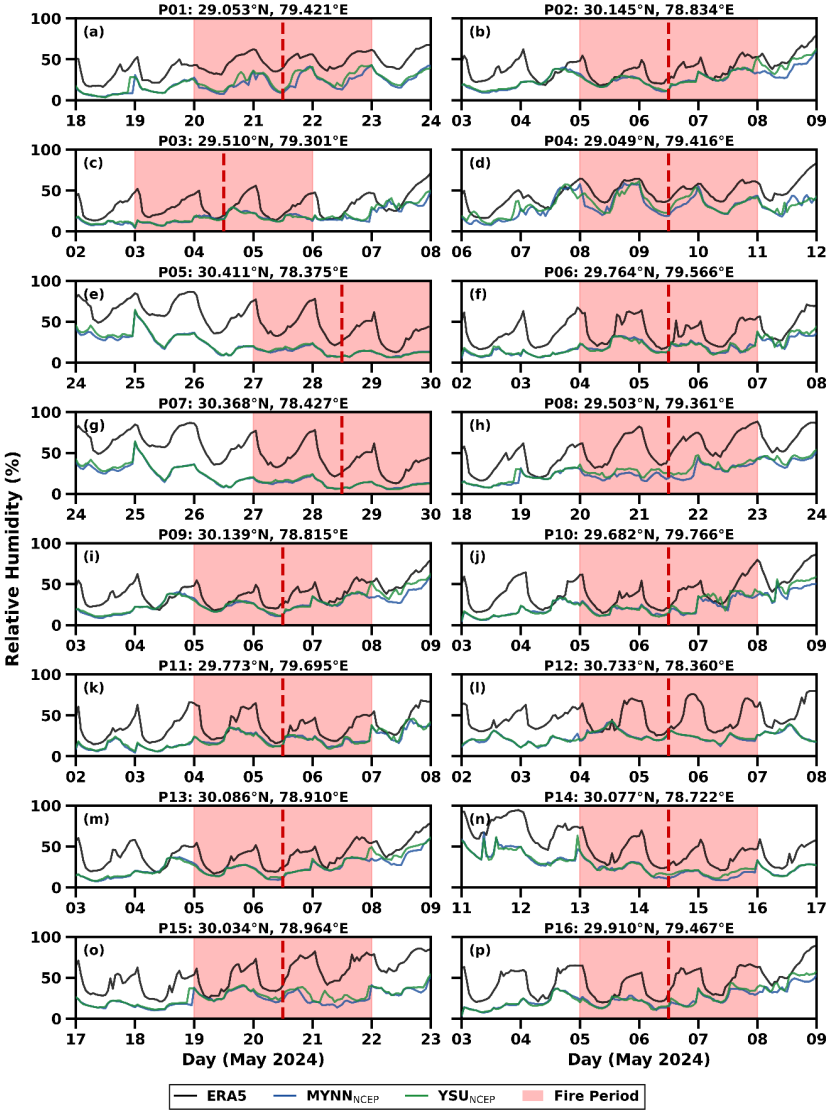

Figure 4 This figure shows the variation in relative humidity (in %) across the 16 major fire clusters. The red shaded region represents the fire period window, with the dotted line representing fire detection

https://doi.org/10.5194/egusphere-2026-2474
Preprint. Discussion started: 6 July 2026
© Author(s) 2026. CC BY 4.0 License.

by the satellite sensors. ERA5 – Land reference, MYNN, and YSU simulations are represented in the respective plots.

Variable	Metric	MYNN	YSU
Relative Humidity	Mean R	0.653	0.659
	Mean IOA	0.586	0.612
	Mean RMSE (%)	24.45	23.25
	Mean Bias (%)	-21.15	-19.77
PBLH	Mean R	0.832	0.900
	Mean IOA	0.817	0.904
	Mean RMSE (m)	888	565
	Mean Bias (m)	+595	+116
Wind Speed (m/s)	Mean R	0.439	0.443
	Mean IOA	0.390	0.385
	Mean RMSE (m s^{-1})	2.15	2.20
	Mean Bias (m s^{-1})	+1.75	+1.81
Sensible Heat Flux	Mean R	0.958	0.961
	Mean IOA	0.964	0.964
	Mean RMSE (W m^{-2})	47.6	48.1
	Mean Bias (W m^{-2})	+1.10	+3.60
Vapour Pressure Deficit	Mean R	0.884	0.892
	Mean IOA	0.804	0.819
	Mean RMSE (kPa)	0.911	0.857
	Mean Bias (kPa)	+0.748	+0.692
FWI	Mean R	0.509	0.591
	Mean IOA	0.460	0.522

https://doi.org/10.5194/egusphere-2026-2474
Preprint. Discussion started: 6 July 2026
© Author(s) 2026. CC BY 4.0 License.

	Mean RMSE	21.50	18.59
	Mean Bias	+19.30	+16.44

Table 4 Summary validation statistics for relative humidity, planetary boundary layer height, sensible heat flux, vapour pressure deficit, and fire weather index with WRF simulations using MYNN and YSU – PBL schemes across the identified fire clusters.

3.2 Wind Speed and Surface Sensible Heat Flux

Wind speed remains another critical factor affecting the spread of fires post-ignition. The wind speed at 10 m remains the least performing fire weather variable across the WRF simulation, with mean R values of 0.435 for $MYNN_{NCEP}$ and 0.443 for YSU_{NCEP}, and the mean IOA remains ~0.4 in both simulations. A systematic positive bias of +1.81 for $MYNN_{NCEP}$ and +1.75 for YSU_{NCEP}. Both experiments used Revised MM5 surface layer schemes, providing insights that near-surface wind speed is strongly controlled by mesoscale circulations and terrain representation within the model. The consistent positive bias in the wind speed was observable across the fire clusters, suggesting that the subgrid orographic drag is not fully parameterised at a 1 km resolution. In-depth analysis of fire clusters revealed contrasting and, in certain cases, similar fire weather characteristics. Fire scenarios at P01, P03, P05, P06, P07, P10, P13, P11, P13, P15 and P16 show increased wind speed values prior to and during the fire weather event (Figure 5). P01 corresponds to the SW-facing slope with consistently increased wind speed values. However, exceptional cases with the north- and northeast-facing slopes (P05, P06, P07, and P15) convey slightly increased wind speed values with lower fire counts, and the wind speed remains relatively lower after the fire weather scenarios. Fire clusters such as P04 and P11 (south-facing slopes) indicated consistently higher wind speeds and postfire weather events.

Surface sensible heat flux (HFX) is another factor that enhances near-surface heating and drives buoyant plume development in wildland fire dynamics (Muth et al., 2025; Trentmann et al., 2006). The enhanced heating from the near–surface increases boundary-layer instability and further promotes vertical mixing, resulting in an elevated PBLH. Thus, the deepened boundary layer increases the fire-atmosphere coupling, accelerating fire spread and intensity through a continuous feedback system (Clark et al., 1996; Linn et al., 2005; Sun et al., n.d.). The HFX simulation remains the best represented variable in both PBL schemes, with both schemes achieving $R > 0.9$, IOA > 0.9, and Nash-Sutcliffe efficiency (NSE) values exceeding 0.8 across all fire clusters (Figure 5) in both simulations. Although the variations were relatively lower, the RMSE and mean bias remained relatively lower for $MYNN_{NCEP}$ than for the YSU_{NCEP} simulations.

https://doi.org/10.5194/egusphere-2026-2474
Preprint. Discussion started: 6 July 2026
© Author(s) 2026. CC BY 4.0 License.

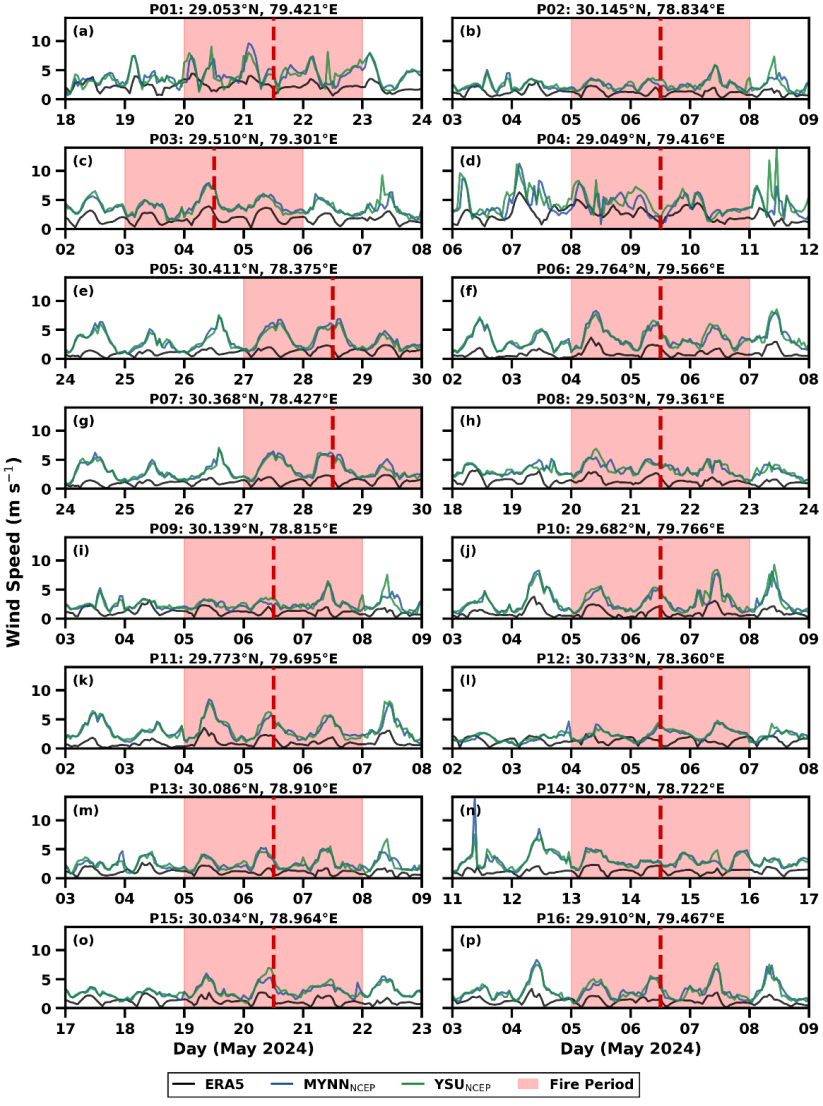

335 **Figure 5** This figure shows the variation in wind speed (in m/s) across the 16 major fire clusters. The red shaded region represents the fire period window, with the dotted line representing fire detection by the satellite sensors. ERA5 - Land reference, MYNN, and YSU simulations are represented in the respective plots.

https://doi.org/10.5194/egusphere-2026-2474
Preprint. Discussion started: 6 July 2026
© Author(s) 2026. CC BY 4.0 License.

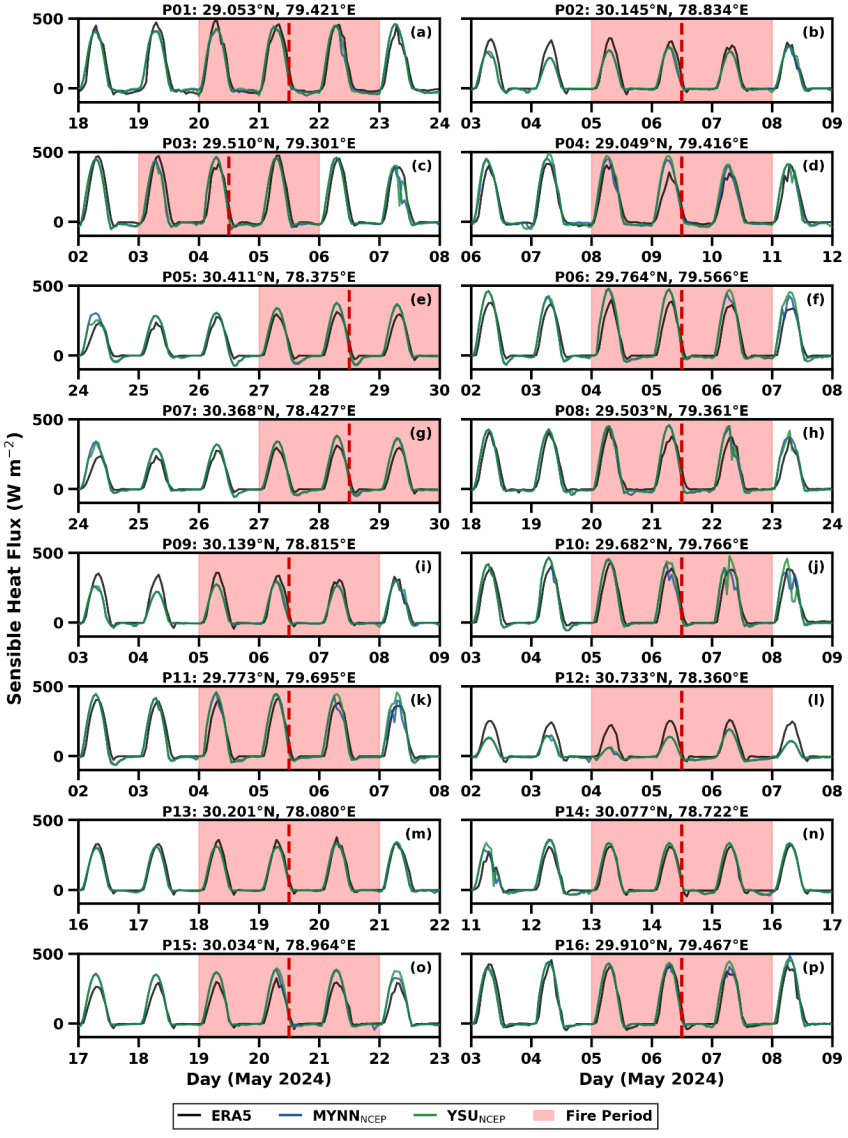

Figure 6 This figure shows the variation in sensible heat flux (in W/m^2) across the 16 major fire clusters. The red shaded region represents the fire period window, with the dotted line representing fire detection by the satellite sensors. ERA5 - Land reference, MYNN, and YSU simulations are represented in the respective plots.

3.3 Planetary Boundary Layer Height

Apart from the basic meteorological variables, the PBLH determines the vertical extent over which the surface-generated heat, moisture and aerosols are mixed into the lower troposphere, thereby governing the fire weather intensity. The height of the PBL is found to vary from 100 to 3000 m, which varies with time, location, local meteorological conditions, and solar radiation acting as a major factor influencing near-surface turbulence. Fire events under increased solar insolation with reduced moisture promote the growth of the PBL, which often reaches a depth of 2 to 4 km (Seibert et al., 2000). PBLH

https://doi.org/10.5194/egusphere-2026-2474
Preprint. Discussion started: 6 July 2026
© Author(s) 2026. CC BY 4.0 License.

simulations from the YSU_{NCEP} and $MYNN_{NCEP}$ resulted in contrasting variations in the statistics. $MYNN_{NCEP}$ overestimated the PBLH with a mean bias value of +595 meters and a mean RMSE of +888 m and an NSE of –0.039, which indicates low predictive skill with the ERA5 reference, whereas YSU_{NCEP} closely aligned with the ERA5 reference, producing R = 0.90, RMSE = 560 m, IOA = 0.904, mean bias = +116, and mean NSE = +0.568, exhibiting comparatively better predictive skill. Across P01 and P08, adjacent to the high-altitude Himalayan region, the bias in $MYNN_{NCEP}$ remains greater than 900 m. However, across P02 and P09, YSU_{NCEP} underestimated the PBLH with a mean bias of -300 m, possibly due to the inadequate representation of surface atmosphere interaction over the forested slopes.

, The spatial variation in the PBLH during the intense forest fire event day on 21st May 2024 is shown in Figure 7. Both schemes overestimated the PBLH with greater variations compared to ERA5-Land. The early morning 05:30 IST shows a shallow PBLH of approximately 200 to 400 m, and YSU_{NCEP} shows nearly the same pattern with slight variation over the Himalayan terrain, whereas $MYNN_{NCEP}$ shows an elevated PBLH compared to the reference values. The morning convective growth had a significant impact on both simulations, with $MYNN_{NCEP}$ simulations estimating PBLH values in the range of 2500 to 3000 meters. Although YSU_{NCEP} overestimates PBLH at this time frame, the variation remains neutral to slightly positive, which closely aligns with the ERA5-BLH ranging from 500 to 1500., PBLH peaks in the afternoon at 15:30 IST with ERA5-BLH ranging from 2000 to 2650 m (in yellow and green), while $MYNN_{NCEP}$ reaches higher PBLH levels (in brown shade, Figure 7) exceeding 4000 to 5000 meters over the flat hills of the Indo-Gangetic Plains (IGP). Unlike other cases, YSU_{NCEP} also overestimated the PBLH with more moderate afternoon growth. However, over the fire cluster locations, the values are consistent with the mean bias shown in Figure 7 near the Himalayan foothills (pale red, YSU_{NCEP} – ERA5). Moreover, during the evening hours at 18:30 IST, the PBLH began to decrease gradually with respect to the reference ERA5 as well as YSU_{NCEP} as the surface buoyancy flux weakened. However, the PBLH continued to grow in the late evening, with $MYNN_{NCEP}$ failing to capture the late-evening stable layer reformation. YSU_{NCEP}, although positively biased, captured the decay toward the nocturnal stable condition. During the late night at 23:30 IST, both YSU_{NCEP} and the reference ERA5 returned to shallow PBLH, with $MYNN_{NCEP}$ attaining lower levels similar to the 05:30 IST PBLH, confirming that the $MYNN_{NCEP}$ overestimation is mainly restricted to daytime convection driven by the TKE response to peak surface buoyancy forcing during the heatwave active, premonsoon, summer, and fire seasons in 2024.

The spatiotemporal analysis of PBLH values across the fire clusters showed that they remained higher during the fire weather days across P01, marking the highest number of fire events with 23 fire alerts. The fire weather generated by the fires and the southwest-facing slope resulted in turbulent fluxes increasing the PBLH across P01 (Figure 8). Meanwhile, the PBLH remains relatively lower across other cases, with a noticeable spike in the PBLH observed during the fire progression across points P05, P06,

https://doi.org/10.5194/egusphere-2026-2474
Preprint. Discussion started: 6 July 2026
© Author(s) 2026. CC BY 4.0 License.

P07, P09, P10, P14 and P16. The north-facing slopes, notably P02, P05, P06, and P07, reveal a distinct pattern where PBLH remains relatively lower during the fire-free period, with PBLH showing significant spikes within the fire weather duration.

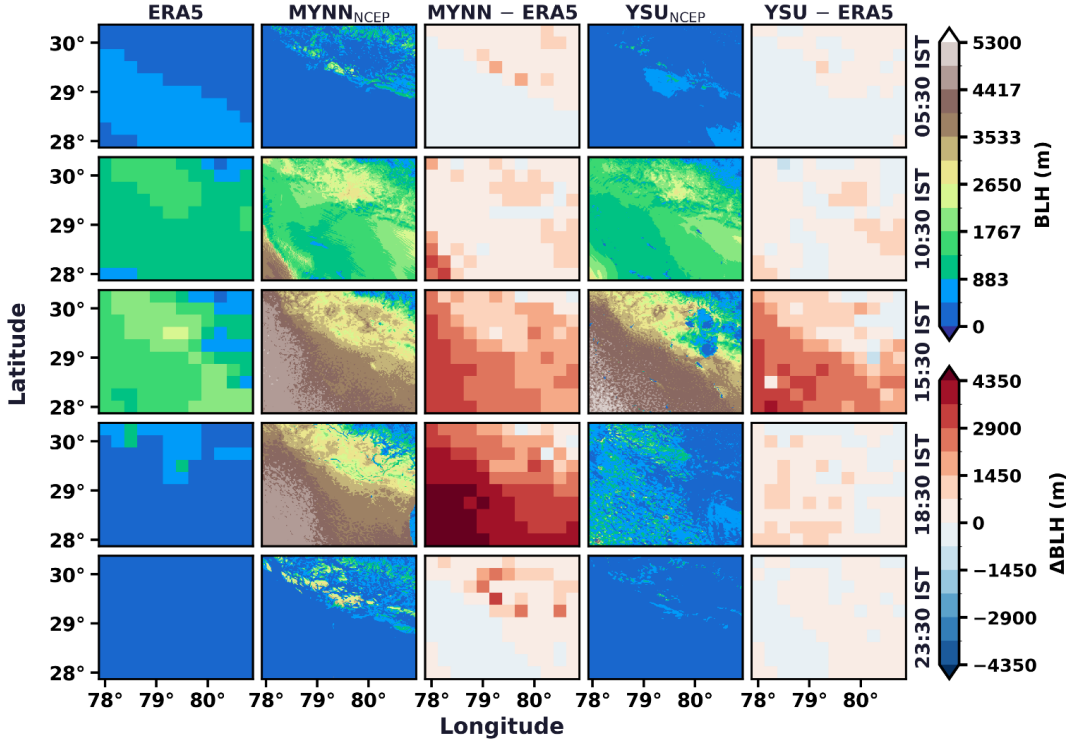

Figure 7 The figure shows the spatial variation in the planetary boundary layer height (in meters) at different Indian standard times (ISTs). The first column is the reference ERA5 data, the second column (MYNN$_{NCEP}$) represents the D02 simulation, the third column represents the difference between the MYNN simulation and the ERA5 reference, the fourth column represents the YSU$_{NCEP}$ simulation, and the fifth column represents the YSU – ERA5 reference.

https://doi.org/10.5194/egusphere-2026-2474
Preprint. Discussion started: 6 July 2026
© Author(s) 2026. CC BY 4.0 License.

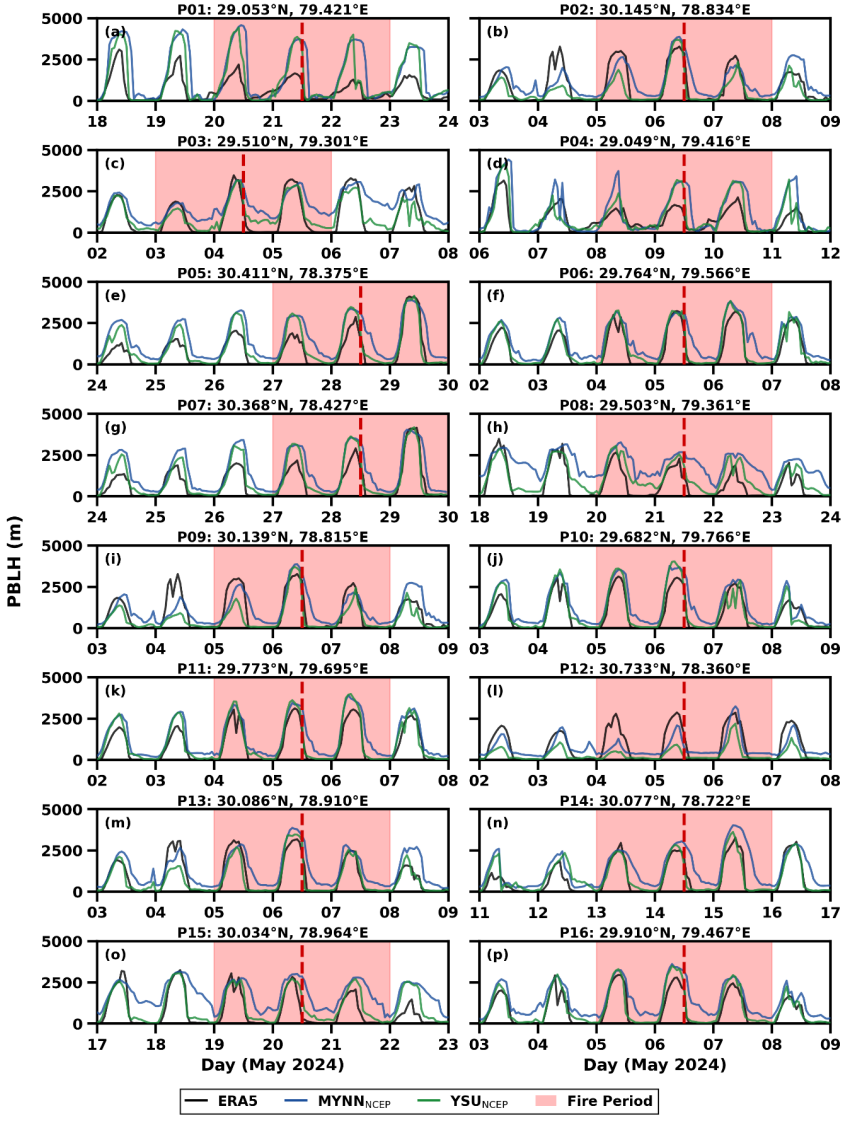

Figure 8 This figure shows the variation in planetary boundary layer height (in m) across the 16 major fire clusters. The red shaded region represents the fire period window, with the dotted line representing fire detection by the satellite sensors. ERA5 - Land reference, MYNN, and YSU simulations are represented in the respective plots.

3.4 Application of the NWP model across the data-sparse region

The validation of multiple meteorological variables suggested that both schemes exhibit similar statistical scores over the Indian Himalayan states. When comparing the 2 m temperature, YSU$_{NCEP}$ performs comparatively better, which may be attributed to the YSU scheme's nonlocal counter gradient transport term that redistributes the heat upwards from the surface more efficiently than MYNN's local TKE closure, which predicts slightly lower temperature values consistent with the reduced warm bias across both regions. The consistent warm biases from the simulation may further be associated with the

https://doi.org/10.5194/egusphere-2026-2474
Preprint. Discussion started: 6 July 2026
© Author(s) 2026. CC BY 4.0 License.

model's capability to overestimate the shortwave surface insulations under anticyclonic pre-monsoon conditions. Furthermore, the model's limitation in resolving subgrid cooler air pooling at a resolution of 1 km over the narrow Himalayan valley suppresses the nocturnal temperature minimum. Such biases alone may not be attributed to PBL schemes; these biases arise from the complex Himalayan topography itself, along with the feedback resulting from the fire weather environment.

Across 16 fire clusters, the fire events initiated at the lowest RH values, asserting the validity of the modelled outputs to simulate the dry weather conditions conducive to forest fire events. The dry bias in the RH is directly related to the 2 m temperature positive mean bias discussed earlier. The elevated temperature increases the saturation vapour pressure, which reduces the RH, resulting in bias values greater than expected over the study domain. Across the HFX simulation, both schemes reproduced similar statistical skill scores across the fire clusters, where the parameterisation schemes used for the simulations with Unified Noah LSM and Revised MM5 surface layer modulate their influence on near-surface temperature gradients and stability. The $MYNN_{NCEP}$ simulations possess a mean bias of 1.10 W/m^2 lower than that of YSU_{NCEP}, with a mean bias of 3.6 W/m^2. However, both the MYNN and YSU simulations were able to capture the HFX diurnal and nocturnal variations without significant variations, which was unexpected over the complex Himalayas. As the simulations proceeded further, $MYNN_{NCEP}$ PBLH simulations resulted in increased PBLH values, while YSU_{NCEP} simulations resulted in values resembling the ERA5 reference. However, statistical skill scores across the basic meteorological variables remain nearly the same with meagre bias over the study area.

Although temperature observations were recorded at 98 stations across the Himalayan states, the datasets may/may not represent the fire zone cluster weather conditions, which resulted in the utilisation of reanalysis datasets for fire cluster analysis. Both the YSU_{NCEP} and $MYNN_{NCEP}$ simulations resulted in statistical skill scores comparatively similar to the mean bias, index of agreement, correlation coefficient and RMSE to remain closer to the reference dataset. This leads to insights into utilising numerical weather prediction models such as WRF in simulating the fire weather conditions associated with the 2024 North Indian fires. The analysed parameters are further used to calculate probable fire spread parameters and fire weather indicators, including VPD and FWI, in the following subsections.

3.5 Vapour Pressure Deficit

Fuel desiccation and fire-prone environments govern the potential for the spread of fires post-ignition. VPD predicts the atmospheric moisture demand and determines the evaporative losses from vegetation and the rapid drying of fuels, which increases the surface fuel flammability. VPD is governed by RH and air temperature, and any variations in their estimation result in overestimating/underestimating the effective VPD. Across the simulations, both schemes perform relatively similarly. YSU_{NCEP} simulations performed comparatively better, capturing the diurnal variations and the associated drying of the atmosphere. As the YSU_{NCEP} and $MYNN_{NCEP}$ simulations

https://doi.org/10.5194/egusphere-2026-2474
Preprint. Discussion started: 6 July 2026
© Author(s) 2026. CC BY 4.0 License.

overestimated the RH and 2 m temperature, this resulted in overestimation spikes in the observed VPD variation. However, except for P01 (Figure 9), all the other fire zones depict negligible variations. P01, located within the Tanda Forest Range, Uttarakhand, faced significant forest fires in the year 2024 with prolonged dry conditions, and the RMSE, mean bias, IOA, and R skill scores increased significantly by a factor greater than 0.1 when considering P02 to P16 alone. Statistical scores for the performed simulations are summarised in Table 4. P01 shows an elevated VPD with dry conditions conducive to the spread of fires. As mentioned before, the combined RH and temperature bias escalated the errors across the schemes. The reference ERA5 suggests extreme fire-prone conditions with VPD values in the range of ~5 to ~7 kPa, similar to the YSU_{NCEP} and $MYNN_{NCEP}$ simulations, which resemble extreme dry conditions. While other locations predict similar values within the admissible range of VPD, P01 remains a critical fire zone with overshooting VPD values during extensive fire events. VPD variations across the fire clusters show a varying pattern, with VPD indicating values similar to extreme fire-conducive environments at P01. The south-facing slope with relatively lower RH and increased temperature and solar radiation results in increased VPD across the Tanda forest range (P01) in Uttarakhand, India. However, across the majority of the fire clusters, VPD values were relatively within the range of dry to extreme dry conditions conducive to the spread of fires.

https://doi.org/10.5194/egusphere-2026-2474
Preprint. Discussion started: 6 July 2026
© Author(s) 2026. CC BY 4.0 License.

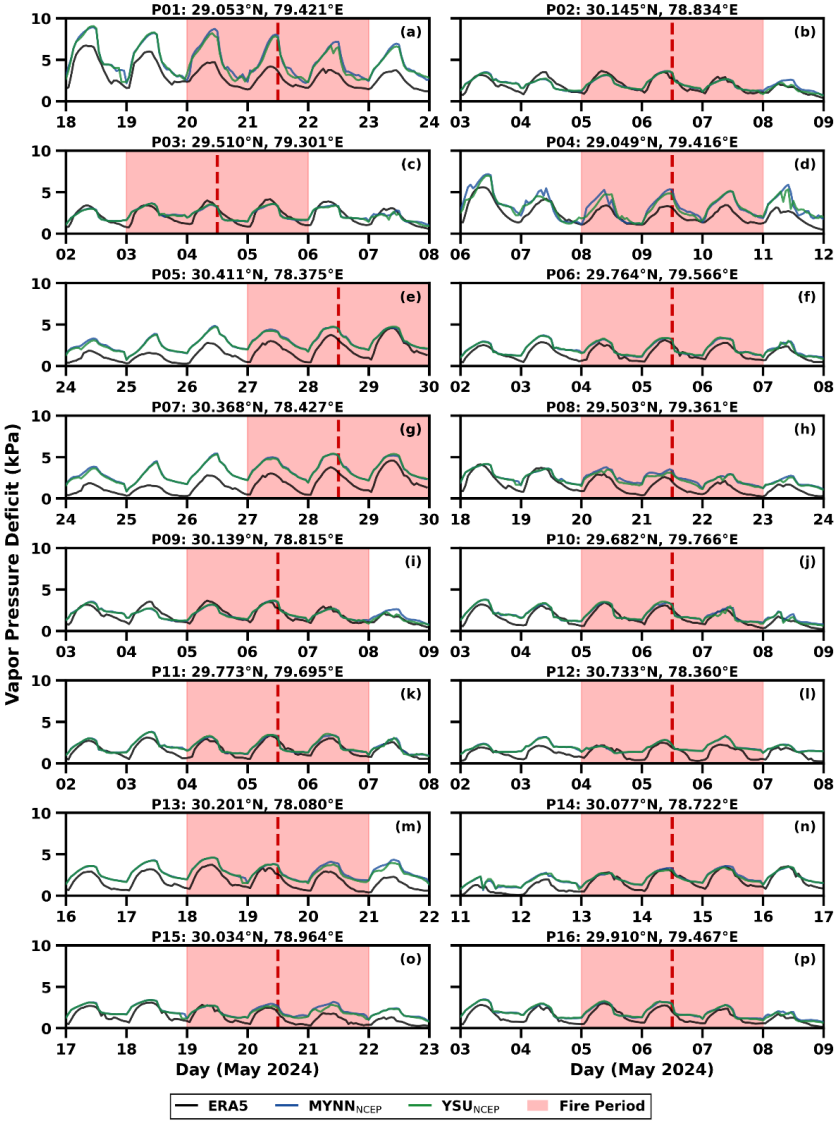

Figure 9 This plot shows the variation in vapour pressure deficit (in kPa) across the 16 major fire clusters. The red shaded region represents the fire period window, with the dotted line representing fire detection by the satellite sensors. ERA5 – Land VPD, MYNN, and YSU simulated VPD are represented in the respective plots.

3.6 Fire Weather Index

Canadian FWI over the Northwest Himalayan region shows significant variation across the 16 fire clusters. Across the study area, the YSU$_{NCEP}$ mean R remains 0.591, mean IOA = 0.522, mean RMSE = 18.59 and mean bias = +16.44, while for MYNN$_{NCEP}$, the values are R = 0.501, mean IOA = 0.460, mean RMSE = 21.50, and mean bias = +19.30. The ERA5-reference FWI ranges from ~7 to ~50, showing a gradient from relatively moderate fire danger in the low elevation zone to increasing danger in the moderate to high altitude Uttarakhand fire cluster across the state of Uttarakhand. MYNN$_{NCEP}$

https://doi.org/10.5194/egusphere-2026-2474
Preprint. Discussion started: 6 July 2026
© Author(s) 2026. CC BY 4.0 License.

produced mean FWI in the range of 22 to 66, while YSU_{NCEP} generated FWI in the mean range of ~ 20 to ~60. Fire clusters P01, P05 and P07 show an increased FWI across all the datasets, with YSU_{NCEP} and $MYNN_{NCEP}$ reaching values greater than 50. At P02, P09, and P12 show lower FWI with fire events claiming the occurrence of fires event at lower FWI. Such lower FWI fires are better represented by the WRF simulations, while the large fire events noticeable over P01 are overestimated by the model. Such nonlinear compound structures of the index system point to the basic indexing within the FWI system with FFMC's strong response towards RH and noon temperature. The ISI scales multiply with the FFMC and wind speed, and the FWI amplifies the ISI through the BUI. Thus, the mean bias accumulation from the temperature, RH and wind speed, along with the precipitation, propagates in the same direction, resulting in the overestimation of the FWI. As the FWI is not standardised over the Indian region, this study uses FWI as a proxy to identify the fire weather conditions without defining an upper bound. The occurrence of fires at lower FWI compared to the higher FWI in P01 raises concern regarding the existing FWI and its application across the tropical region, regarding the representation of solar radiation and tropical region-specific inputs to the existing FWI.

https://doi.org/10.5194/egusphere-2026-2474
Preprint. Discussion started: 6 July 2026
© Author(s) 2026. CC BY 4.0 License.

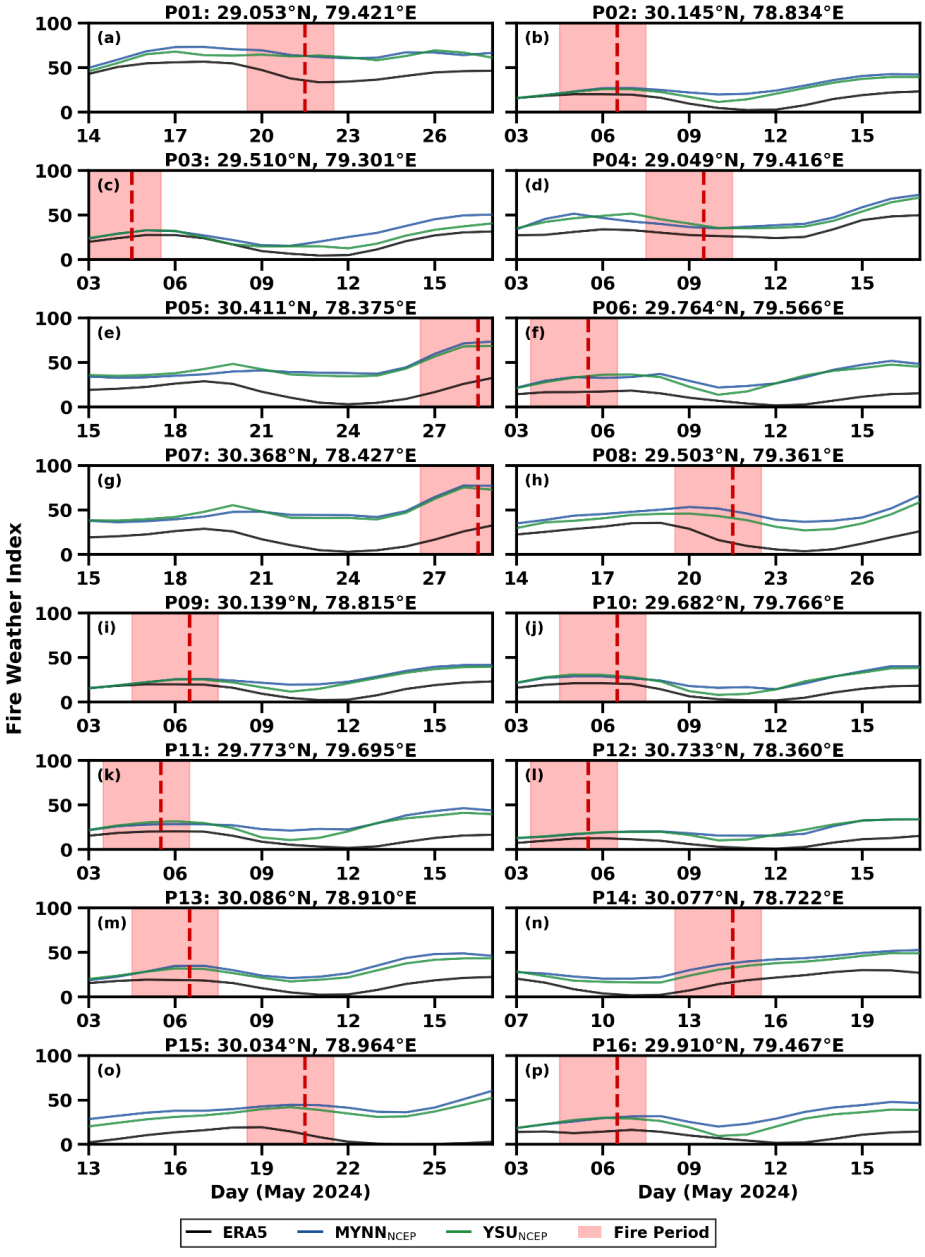

Figure 10 This figure shows the variation in the Fire Weather Index across 16 major fire clusters. The red shaded region represents the fire period window, with the dotted line representing fire detection by the satellite sensors. ERA5 – Land FWI, MYNN, and YSU simulated FWI are represented in the respective plots.

4 Conclusion

This study elaborates on a systematic evaluation of suitable PBL schemes for simulating fire weather conditions conducive to the spread of wildfires over the Indian Himalayan states of Uttarakhand and Himachal Pradesh. The majority of the meteorological variables generated similar

https://doi.org/10.5194/egusphere-2026-2474
Preprint. Discussion started: 6 July 2026
© Author(s) 2026. CC BY 4.0 License.

statistical scores for 2 m temperature, relative humidity, wind speed, and surface sensible heat flux. However, PBLH values were abnormally higher for the $MYNN_{NCEP}$ during the 18:30 IST time across the lower portion of the Indo – Gangetic Plains, which do not coincide with the fire cluster zones. The PBLH over the fire clusters remains nearly the same across both the $MYNN_{NCEP}$ and YSU_{NCEP} simulations. As the statistical skill scores were relatively better across the fire clusters, the model simulations may be utilised as a proxy over the Himalayan region to determine the fire weather evolution across the fire clusters.

The majority of the fire clusters were located on the south-facing slopes compared to the north-facing slopes, where solar insolation increases the dryness across the south compared to the north, and surface moisture remains relatively higher on the north-facing slopes due to relatively lower solar radiation reaching the surface. However, fires were noticeable over the north-facing slope with considerably lower wind speeds compared to the south-facing slope surfaces. RH remains relatively drier across the study area with a warm dry bias, and the temperature values remain significantly higher during fire weather events. During the fire events, the PBLH value shows a spike during and postfire initiation due to the fire near-surface turbulence that is perfectly captured by the WRF model simulations. The sensible heat flux values remain relatively similar and possess near-perfect correlation across the simulated scenarios. Fire weather indicators, including VPD and FWI values, were relatively higher, with the Tanda forest range, Uttarakhand possessing extremely dry weather conditions susceptible to the spread of fires. VPD values except P01 resemble the VPD study by Prabhakaran & Srivastava, (2024) over the North Indian region, denoting fire-prone conditions being accurately represented by the simulations. A pattern of peak FWI value clusters being susceptible to fires is clearly simulated across all the fire clusters. The FWI indices fall short at locations where lower FWI responses correspond to fire events. FWI values beyond the fire date may not be used for forecasting, as the fire scenarios have eradicated the surface fuels across the area.

As the Himalayan region is prone to several fires on an annual basis, with the increasing number of winter wildfires, this study extends the application of the NWP model as a proxy over the data-sparse tropical region for simulating atmospheric conditions conducive to forest fires. The appropriate incorporation of solar radiation, alignment of slope and regional-specific topographical data and drying factor in the drought code (part of FWI) into the fire weather indices may accurately reflect the fire weather conditions over the Indian region. Furthermore, this study may be coupled with a suitable fire module, such as WRF-FIRE or WRF-SFire, to couple the impact of fire weather to predict the fire-induced behaviour and the evolution of fires in the tropical Himalayas under the changing climate, which enhances the early fire danger rating system for the vulnerable population in the Himalayan foothills.

Code and Data Availability

https://doi.org/10.5194/egusphere-2026-2474
Preprint. Discussion started: 6 July 2026
© Author(s) 2026. CC BY 4.0 License.

All the codes used for the study may be available upon request. An observational dataset from the India Meteorological Department is used in the study. The NCEP-FNL dataset used as the initial and boundary conditions for the WRF model is available at https://gdex.ucar.edu/datasets/d083002/. The validation dataset of ERA5 is available at https://doi.org/10.24381/cds.adbb2d47, and ERA5-Land is available at https://doi.org/10.24381/cds.e2161bac.

Supplement

The supplement related to the article is available along with the Manuscript.

Author Contributions

AP conceived the study, carried out the model setup and simulations, performed the postprocessing and detailed analysis of the results, and led the manuscript preparation and editing. PS contributed to the conceptualisation of the study and supported the manuscript preparation, writing, editing and supervision.

Competing interests

The authors declare that there are no existing conflicts of interest for this manuscript.

Acknowledgements

The authors would like to acknowledge PARAMGANGA - Supercomputing facility of IIT Roorkee, established under the National Supercomputing Mission (NSM) Phase II, Government of India. AP acknowledges the support from the Centre of Excellence in Disaster Mitigation and Management, Indian Institute of Technology Roorkee, India and Ministry of Education, Government of India via Prime Minister's Research Fellowship program with Grant no: 2802864 for funding this study. AP would like to thank Ms. Anamika Sekar for the useful discussion. The authors acknowledge the support from the India Meteorological Department for providing the AWS dataset across the study domain.

Financial Support

AP acknowledges the support from the Ministry of Education, Government of India via Prime Minister's Research Fellowship program with Grant no: 2802864 for funding this study.

References

Abatzoglou, J. T., Kolden, C. A., Cullen, A. C., Sadegh, M., Williams, E. L., Turco, M., & Jones, M. W. (2025). Climate change has increased the odds of extreme regional forest fire years globally. *Nature Communications* , *16*(1). https://doi.org/10.1038/s41467-025-61608-1

Ager, A. A., Vaillant, N. M., & Finney, M. A. (2011). Integrating fire behavior models and geospatial analysis for wildland fire risk assessment and fuel management planning. *Journal of Combustion*, *2011*. https://doi.org/10.1155/2011/572452

Andrews, P. L., & Bevins, C. D. (2003). BehavePlus fire modeling system, version 2: overview. *2nd International Wildland Fire Ecology and Fire Management Congress; November 16-20, 2003*.

Andrews, P. L., Bevins, C. D., & Seli, R. C. (2005). BehavePlus fire modeling system version 3.0 user's guide. *USDA Forest Service - General Technical Report RMRS-GTR*, (106 RMRS-GTR).

https://doi.org/10.5194/egusphere-2026-2474
Preprint. Discussion started: 6 July 2026
© Author(s) 2026. CC BY 4.0 License.

Athira, K. S., Roxy, M. K., Dasgupta, P., Saranya, J. S., Singh, V. K., & Attada, R. (2023). Regional and temporal variability of Indian summer monsoon rainfall in relation to El Niño southern oscillation. *Scientific Reports*, *13*(1). https://doi.org/10.1038/s41598-023-38730-5

Bhattacharyya, S., Hassan, M. A., Sreekesh, S., & Choudhary, V. (2025). How well do the reanalysis datasets capture hot and cold extremes and their trends in India? *Atmospheric Research*, *321*. https://doi.org/10.1016/j.atmosres.2025.108073

Bhattarai, H., Val Martin, M., Sitch, S., Yung, D. H. Y., & Tai, A. P. K. (2025). Global wildfire patterns and drivers under climate change. *Biogeosciences*, *22*(23). https://doi.org/10.5194/bg-22-7591-2025

Burton, C., Betts, R. A., Jones, C. D., Feldpausch, T. R., Cardoso, M., & Anderson, L. O. (2020). El Niño Driven Changes in Global Fire 2015/16. *Frontiers in Earth Science*, *8*, 199. https://doi.org/10.3389/FEART.2020.00199/BIBTEX

Carta, F., Zidda, C., Putzu, M., Loru, D., Anedda, M., & Giusto, D. (2023). Advancements in Forest Fire Prevention: A Comprehensive Survey. In *Sensors* (Vol. 23, Number 14). https://doi.org/10.3390/s23146635

Clark, T. L., Jenkins, M. A., Coen, J., & Packham, D. (1996). A coupled atmosphere-fire model: Convective feedback on fire-Line dynamics. *Journal of Applied Meteorology*, *35*(6). https://doi.org/10.1175/1520-0450(1996)035<0875:ACAMCF>2.0.CO;2

Coen, J. L., Cameron, M., Michalakes, J., Patton, E. G., Riggan, P. J., & Yedinak, K. M. (2013). Wrf-fire: Coupled weather-wildland fire modeling with the weather research and forecasting model. *Journal of Applied Meteorology and Climatology*, *52*(1), 16–38. https://doi.org/10.1175/JAMC-D-12-023.1

Cohen, A. E., Cavallo, S. M., Coniglio, M. C., & Brooks, H. E. (2015). A review of planetary boundary layer parameterization schemes and their sensitivity in simulating southeastern U.S. cold season severe weather environments. In *Weather and Forecasting* (Vol. 30, Number 3). https://doi.org/10.1175/WAF-D-14-00105.1

Cruz, M. G., & Alexander, M. E. (2013). Uncertainty associated with model predictions of surface and crown fire rates of spread. *Environmental Modelling and Software*, *47*. https://doi.org/10.1016/j.envsoft.2013.04.004

Di Giuseppe, F., Pappenberger, F., Wetterhall, F., Krzeminski, B., Camia, A., Libertá, G., & Miguel, J. S. (2016). The potential predictability of fire danger provided by numerical weather prediction. *Journal of Applied Meteorology and Climatology*, *55*(11), 2469–2491. https://doi.org/10.1175/JAMC-D-15-0297.1

Di Giuseppe, F., Vitolo, C., Krzeminski, B., Barnard, C., MacIel, P., & San-Miguel, J. (2020). Fire Weather Index: The skill provided by the European Centre for Medium-Range Weather Forecasts ensemble prediction system. *Natural Hazards and Earth System Sciences*, *20*(8), 2365–2378. https://doi.org/10.5194/nhess-20-2365-2020

Finney, M. A. (1998). FARSITE: Fire Area Simulator - Model Development and Evaluation. *USDA Forest Service - Research Papers RMRS*, (RMRS-RP-4).

Flannigan, M. D., Krawchuk, M. A., De Groot, W. J., Wotton, B. M., & Gowman, L. M. (2009). Implications of changing climate for global wildland fire. In *International Journal of Wildland Fire* (Vol. 18, Number 5). https://doi.org/10.1071/WF08187

Forest Survey of India. (2021). *Van Agni Geo-portal*. Last Access: 14 November 2025. https://vanagniportal.fsiforestfire.gov.in/

FSI. (2019). *[Forest Survey of India], India State of Forest Report*. https://fsi.nic.in/isfr2019/isfr-fsi-vol2.pdf

FSI. (2021). *[Forest Survey of India], India State of Forest Report*. https://fsi.nic.in/forest-report-2021-details

FSI. (2023). *[Forest Survey of India], India State of Forest Report*. https://fsi.nic.in/uploads/isfr2023/isfr_book_eng-vol-1_2023.pdf

Gilliam, R. C., & Pleim, J. E. (2010). Performance assessment of new land surface and planetary boundary layer physics in the WRF-ARW. *Journal of Applied Meteorology and Climatology*, *49*(4). https://doi.org/10.1175/2009JAMC2126.1

https://doi.org/10.5194/egusphere-2026-2474
Preprint. Discussion started: 6 July 2026
© Author(s) 2026. CC BY 4.0 License.

Gohm, A., Zängl, G., & Mayr, G. J. (2004). South Foehn in the Wipp Valley on 24 October 1999 (MAP IOP 10): Verification of high-resolution numerical simulations with observations. *Monthly Weather Review*, *132*(1). https://doi.org/10.1175/1520-0493(2004)132<0078:SFITWV>2.0.CO;2

Griffin, S. M., & Otkin, J. A. (2022). Evaluating the Impact of Planetary Boundary Layer, Land Surface Model, and Microphysics Parameterization Schemes on Simulated GOES-16 Water Vapor Brightness Temperatures. *Atmosphere*, *13*(3). https://doi.org/10.3390/atmos13030366

Hersbach, H. , Bell, B. , Berrisford, P. , Biavati, G. , Horányi, A. , Muñoz Sabater, J. , Nicolas, J. , Peubey, C. , Radu, R. , Rozum, I. , Schepers, D. , Simmons, A. , Soci, C. , Dee, D. , & Thépaut, J.-N. (2023). ERA5 hourly data on single levels from 1940 to present. Copernicus Climate Change Service (C3S) Climate Data Store (CDS), DOI: 10.24381/cds.adbb2d47 (Accessed on 01-Nov-2025). *Ecmwf*, *147*.

Hersbach, H., Bell, B., Berrisford, P., Hirahara, S., Horányi, A., Muñoz-Sabater, J., Nicolas, J., Peubey, C., Radu, R., Schepers, D., Simmons, A., Soci, C., Abdalla, S., Abellan, X., Balsamo, G., Bechtold, P., Biavati, G., Bidlot, J., Bonavita, M., … Thépaut, J. N. (2020). The ERA5 global reanalysis. *Quarterly Journal of the Royal Meteorological Society*, *146*(730). https://doi.org/10.1002/qj.3803

Hoffman, K. M., Christianson, A. C., Gray, R. W., & Daniels, L. (2022). Western Canada's new wildfire reality needs a new approach to fire management. *Environmental Research Letters*, *17*(6). https://doi.org/10.1088/1748-9326/ac7345

Holsinger, L., Parks, S. A., & Miller, C. (2016). Weather, fuels, and topography impede wildland fire spread in western US landscapes. *Forest Ecology and Management*, *380*. https://doi.org/10.1016/j.foreco.2016.08.035

Hong, S. Y., Noh, Y., & Dudhia, J. (2006). A new vertical diffusion package with an explicit treatment of entrainment processes. *Monthly Weather Review*, *134*(9). https://doi.org/10.1175/MWR3199.1

Hu, X. M., Klein, P. M., & Xue, M. (2013). Evaluation of the updated YSU planetary boundary layer scheme within WRF for wind resource and air quality assessments. *Journal of Geophysical Research Atmospheres*, *118*(18). https://doi.org/10.1002/jgrd.50823

Hunt, K. M. R., Baudouin, J. P., Turner, A. G., Dimri, A. P., Jeelani, G., Pooja, Chattopadhyay, R., Cannon, F., Arulalan, T., Shekhar, M. S., Sabin, T. P., & Palazzi, E. (2025). Western disturbances and climate variability: A review of recent developments. In *Weather and Climate Dynamics* (Vol. 6, Number 1, pp. 43–112). Copernicus Publications. https://doi.org/10.5194/wcd-6-43-2025

Hunt, K. M. R., Turner, A. G., & Shaffrey, L. C. (2019). Falling trend of western disturbances in future climate simulations. *Journal of Climate*, *32*(16), 5037–5051. https://doi.org/10.1175/JCLI-D-18-0601.1

Hunt, K. M. R., & Zaz, S. N. (2023). Linking the North Atlantic Oscillation to winter precipitation over the Western Himalaya through disturbances of the subtropical jet. *Climate Dynamics*, *60*(7–8), 2389–2403. https://doi.org/10.1007/s00382-022-06450-7

India Meteorological Department (IMD). (2024a). *Current Weather Status and Extended Range Forecast for Next Two Weeks (30 May–12 June 2024)*. https://internal.imd.gov.in/press_release/20240603_pr_3037.pdf

India Meteorological Department (IMD). (2024b). *Heat wave to severe heat wave conditions likely to continue over plains of Northwest India during next 5 days and Heat wave conditions likely over East & Central India during next 3 days*. http://internal.imd.gov.in/press_release/20240518_pr_3004.pdf

India Meteorological Department (IMD). (2024c). *Prevailing heat wave to severe heat wave conditions over Northwest & Central India likely to reduce gradually*. https://internal.imd.gov.in/press_release/20240530_pr_3031.pdf

India Meteorological Department (IMD). (2024d). *Prevailing heat wave to severe heat wave conditions over Northwest & Central India likely to reduce gradually from 30th May, 2024*. https://internal.imd.gov.in/press_release/20240528_pr_3025.pdf

https://doi.org/10.5194/egusphere-2026-2474
Preprint. Discussion started: 6 July 2026
© Author(s) 2026. CC BY 4.0 License.

Jain, P., Barber, Q. E., Taylor, S. W., Whitman, E., Castellanos Acuna, D., Boulanger, Y., Chavardès, R. D., Chen, J., Englefield, P., Flannigan, M., Girardin, M. P., Hanes, C. C., Little, J., Morrison, K., Skakun, R. S., Thompson, D. K., Wang, X., & Parisien, M. A. (2024). Drivers and Impacts of the Record-Breaking 2023 Wildfire Season in Canada. *Nature Communications*, *15*(1). https://doi.org/10.1038/s41467-024-51154-7

James, E., Ahmadov, R., Romero-Alvarez, J., Grell, G., Csiszar, I., Anderson, L. D., Schnell, J., & DE GOUW, J. (2025). An Hourly Wildfire Potential Index for Predicting Subdaily Fire Activity Based on Rapidly Updating Convection-Allowing Model Forecasts. *Weather and Forecasting*, *40*(9). https://doi.org/10.1175/WAF-D-24-0068.1

Jin, Y., Randerson, J. T., Faivre, N., Capps, S., Hall, A., & Goulden, M. L. (2014). Contrasting controls on wildland fires in Southern California during periods with and without Santa Ana winds. *Journal of Geophysical Research: Biogeosciences*, *119*(3). https://doi.org/10.1002/2013JG002541

Jones, M. W., Abatzoglou, J. T., Veraverbeke, S., Andela, N., Lasslop, G., Forkel, M., Smith, A. J. P., Burton, C., Betts, R. A., van der Werf, G. R., Sitch, S., Canadell, J. G., Santín, C., Kolden, C., Doerr, S. H., & Le Quéré, C. (2022). Global and Regional Trends and Drivers of Fire Under Climate Change. In *Reviews of Geophysics* (Vol. 60, Number 3). John Wiley and Sons Inc. https://doi.org/10.1029/2020RG000726

Kalogiannidis, S., Kalfas, D., Kontsas, S., Papaevangelou, O., & Chatzitheodoridis, F. (2025). Evaluating the Effectiveness of Early Warning Systems in Reducing Loss of Life in Natural Disasters: A case study of Greece. *Journal of Risk Analysis and Crisis Response*, *15*(1). https://doi.org/10.54560/jracr.v15i1.547

Keeley, J. E. (2004). Impact of antecedent climate on fire regimes in coastal California. *International Journal of Wildland Fire*, *13*(2). https://doi.org/10.1071/WF03037

Khairoutdinov, M., Randall, D., & DeMott, C. (2005). Simulations of the atmospheric general circulation using a cloud-resolving model as a superparameterization of physical processes. *Journal of the Atmospheric Sciences*, *62*(7 I). https://doi.org/10.1175/JAS3453.1

Kumar, M., Kosović, B., Nayak, H. P., Porter, W. C., Randerson, J. T., & Banerjee, T. (2023). Evaluating the performance of WRF in simulating winds and surface meteorology during a Southern California wildfire event. *Frontiers in Earth Science*, *11*. https://doi.org/10.3389/feart.2023.1305124

Lawson, B. D., & Armitage, O. B. (2008). Weather Guide for THE CANADIAN SYSTEM OF FOREST FIRE DANGER RATING. In *Weather* (Number July).

Linn, R., Winterkamp, J., Colman, J. J., Edminster, C., & Bailey, J. D. (2005). Modeling interactions between fire and atmosphere in discrete element fuel beds. *International Journal of Wildland Fire*, *14*(1). https://doi.org/10.1071/WF04043

Mandel, J., Beezley, J. D., & Kochanski, A. K. (2011). Coupled atmosphere-wildland fire modeling with WRF 3.3 and SFIRE 2011. *Geoscientific Model Development*, *4*(3), 591–610. https://doi.org/10.5194/gmd-4-591-2011

Mantovani Júnior, J. A., Aravéquia, J. A., Carneiro, R. G., & Fisch, G. (2023). Evaluation of PBL Parameterization Schemes in WRF Model Predictions during the Dry Season of the Central Amazon Basin. *Atmosphere*, *14*(5). https://doi.org/10.3390/atmos14050850

Måren, I. E., Karki, S., Prajapati, C., Yadav, R. K., & Shrestha, B. B. (2015). Facing north or south: Does slope aspect impact forest stand characteristics and soil properties in a semiarid trans-Himalayan valley? *Journal of Arid Environments*, *121*. https://doi.org/10.1016/j.jaridenv.2015.06.004

Mina, U., Dimri, A. P., & Farswan, S. (2023). Forest fires and climate attributes interact in central Himalayas: an overview and assessment. *Fire Ecology*, *19*(1). https://doi.org/10.1186/s42408-023-00177-4

Mölders, N. (2008). Suitability of the Weather Research and Forecasting (WRF) model to predict the June 2005 fire weather for interior Alaska. *Weather and Forecasting*, *23*(5). https://doi.org/10.1175/2008WAF2007062.1

https://doi.org/10.5194/egusphere-2026-2474
Preprint. Discussion started: 6 July 2026
© Author(s) 2026. CC BY 4.0 License.

Mondal, N., & Sukumar, R. (2014). Characterising weather patterns associated with fire in a seasonally dry tropical forest in southern India. *International Journal of Wildland Fire*, *23*(2). https://doi.org/10.1071/WF13002

Muñoz Sabater, J. (2019). *ERA5-Land hourly data from 1950 to present. Copernicus Climate Change Service (C3S) Climate Data Store (CDS)*. Access on 01 November 2025.

Muth, L. J., Bierbauer, S., Hoose, C., Vogel, B., Vogel, H., & Hoshyaripour, G. A. (2025). Influence of fire-induced heat and moisture release on pyro-convective cloud dynamics during the Australian New Year's Event: A study using convection-resolving simulations and satellite data. *Atmospheric Chemistry and Physics*, *25*(22). https://doi.org/10.5194/acp-25-16027-2025

Nakanishi, M., & Niino, H. (2004). An improved Mellor-Yamada Level-3 model with condensation physics: Its design and verification. *Boundary-Layer Meteorology*, *112*(1). https://doi.org/10.1023/B:BOUN.0000020164.04146.98

NCEP - FNL. (2000). *National Centers for Environmental Prediction/National Weather Service/NOAA/U.S. Department of Commerce (2000): NCEP FNL Operational Model Global Tropospheric Analyses, continuing from July 1999. NSF National Center for Atmospheric Research. Dataset. Accessed 05-June-2025*. NSF National Center for Atmospheric Research. https://doi.org/10.5065/D6M043C6

NDMA. (2021). *National Disaster Management Authority : SACHET – Integrated Alert System, Government of India* . https://sachet.ndma.gov.in/

Nolan, R. H., Boer, M. M., Collins, L., Resco de Dios, V., Clarke, H., Jenkins, M., Kenny, B., & Bradstock, R. A. (2020). Causes and consequences of eastern Australia's 2019–20 season of mega-fires. In *Global Change Biology* (Vol. 26, Number 3, pp. 1039–1041). Blackwell Publishing Ltd. https://doi.org/10.1111/gcb.14987

Ocón, J. P., Ibanez, T., Franklin, J., Pau, S., Keppel, G., Rivas-Torres, G., Edward, M., & Gillespie, T. W. (2021). Global tropical dry forest extent and cover: A comparative study of bioclimatic definitions using two climatic data sets. *PLoS ONE*, *16*(5 May). https://doi.org/10.1371/journal.pone.0252063

Powers, J. G., Klemp, J. B., Skamarock, W. C., Davis, C. A., Dudhia, J., Gill, D. O., Coen, J. L., Gochis, D. J., Ahmadov, R., Peckham, S. E., Grell, G. A., Michalakes, J., Trahan, S., Benjamin, S. G., Alexander, C. R., Dimego, G. J., Wang, W., Schwartz, C. S., Romine, G. S., … Duda, M. G. (2017). The weather research and forecasting model: Overview, system efforts, and future directions. *Bulletin of the American Meteorological Society*, *98*(8). https://doi.org/10.1175/BAMS-D-15-00308.1

Prabhakaran, A., & Srivastava, P. (2024). Analysis of prevailing atmospheric conditions during wildfire events in the Indian Himalayan region. *Quarterly Journal of the Royal Meteorological Society*. https://doi.org/10.1002/qj.4918

Prabhakaran, A., & Srivastava, P. (2026). Impact of El Niño Southern Oscillation and Indian ocean dipole on wildfire across the Indian forests. *Natural Hazards*, *122*(4). https://doi.org/10.1007/s11069-025-07937-2

Prasad, V. K., Badarinath, K. V. S., & Eaturu, A. (2008). Biophysical and anthropogenic controls of forest fires in the Deccan Plateau, India. *Journal of Environmental Management*, *86*(1). https://doi.org/10.1016/j.jenvman.2006.11.017

Price, S. "Jake," & Germino, M. J. (2022). Modeling of fire spread in sagebrush steppe using FARSITE: an approach to improving input data and simulation accuracy. *Fire Ecology*, *18*(1). https://doi.org/10.1186/s42408-022-00147-2

Ruffault, J., Curt, T., Martin-Stpaul, N. K., Moron, V., & Trigo, R. M. (2018). Extreme wildfire events are linked to global-change-type droughts in the northern Mediterranean. *Natural Hazards and Earth System Sciences*, *18*(3). https://doi.org/10.5194/nhess-18-847-2018

Schaefer, M. L., Bogacki, W., Lopez Caceres, M. L., Kirschbauer, L., Kato, C., & Kikuchi, S. I. (2024). Influence of Slope Aspect and Vegetation on the Soil Moisture Response to Snowmelt in the German Alps. *Hydrology*, *11*(7). https://doi.org/10.3390/hydrology11070101

https://doi.org/10.5194/egusphere-2026-2474
Preprint. Discussion started: 6 July 2026
© Author(s) 2026. CC BY 4.0 License.

Seibert, P., Beyrich, F., Gryning, S. E., Joffre, S., Rasmussen, A., & Tercier, P. (2000). Review and intercomparison of operational methods for the determination of the mixing height. In *Atmospheric Environment* (Vol. 34, Number 7). https://doi.org/10.1016/S1352-2310(99)00349-0

Shin, H. H., & Hong, S. Y. (2015). Representation of the subgrid-scale turbulent transport in convective boundary layers at gray-zone resolutions. *Monthly Weather Review*, *143*(1). https://doi.org/10.1175/MWR-D-14-00116.1

Singh, J., Singh, N., Ojha, N., Dimri, A. P., & Singh, R. S. (2024). Impacts of different boundary layer parameterization schemes on simulation of meteorology over Himalaya. *Atmospheric Research*, *298*. https://doi.org/10.1016/j.atmosres.2023.107154

Singh, J., Singh, N., Ojha, N., Sharma, A., Pozzer, A., Kiran Kumar, N., Rajeev, K., Gunthe, S. S., & Rao Kotamarthi, V. (2021). Effects of spatial resolution on WRF v3.8.1 simulated meteorology over the central Himalaya. *Geoscientific Model Development*, *14*(3). https://doi.org/10.5194/gmd-14-1427-2021

Singh, S., & Srivastava, P. (2025). Parameterization of Surface Layer Processes in Extreme Weather Conditions over Mountainous Region. *Weather and Forecasting*. https://doi.org/10.1175/waf-d-24-0178.1

Skamarock WC, et al. (2008). A description of the advanced research WRF version 3, NCAR Tech. Note, NCAR/TN-468+STR. *Natl. Cent. for Atmos. Res. Boulder, Colorado*, (June).

Solomos, S., Kalivitis, N., Mihalopoulos, N., Amiridis, V., Kouvarakis, G., Gkikas, A., Binietoglou, I., Tsekeri, A., Kazadzis, S., Kottas, M., Pradhan, Y., Proestakis, E., Nastos, P. T., & Marenco, F. (2018). From tropospheric folding to Khamsin and Foehn winds: How atmospheric dynamics advanced a record-breaking dust episode in Crete. *Atmosphere*, *9*(7). https://doi.org/10.3390/atmos9070240

Sullivan, A. L. (2009). Wildland surface fire spread modelling, 1990–2007. 3: Simulation and mathematical analogue models. *International Journal of Wildland Fire*, *18*(4). https://doi.org/10.1071/wf06144

Sun, R., Krueger, S. K., Zulauf, M. A., Jenkins, M. A., & Charney, J. J. (n.d.). *WILDFIRE EVOLUTION IN THE CONVECTIVE BOUNDARY LAYER*.

Tang, Y., Lean, H. W., & Bornemann, J. (2013). The benefits of the Met Office variable resolution NWP model for forecasting convection. *Meteorological Applications*, *20*(4). https://doi.org/10.1002/met.1300

Trentmann, J., Luderer, G., Winterrath, T., Fromm, M. D., Servranckx, R., Textor, C., Herzog, M., Graf, H. F., & Andreae, M. O. (2006). Modeling of biomass smoke injection into the lower stratosphere by a large forest fire (Part I): Reference simulation. *Atmospheric Chemistry and Physics*, *6*(12). https://doi.org/10.5194/acp-6-5247-2006

Turco, M., Abatzoglou, J. T., Herrera, S., Zhuang, Y., Jerez, S., Lucas, D. D., AghaKouchak, A., & Cvijanovic, I. (2023). Anthropogenic climate change impacts exacerbate summer forest fires in California. *Proceedings of the National Academy of Sciences of the United States of America*, *120*(25). https://doi.org/10.1073/pnas.2213815120

Vitolo, C., Giuseppe, F. Di, & D'Andrea, M. (2018). Caliver: An R package for CALIbration and VERification of forest fire gridded model outputs. *PLoS ONE*, *13*(1), 1–18. https://doi.org/10.1371/journal.pone.0189419

Xie, B., Fung, J. C. H., Chan, A., & Lau, A. (2012). Evaluation of nonlocal and local planetary boundary layer schemes in the WRF model. *Journal of Geophysical Research Atmospheres*, *117*(12). https://doi.org/10.1029/2011JD017080

Yang, J., El-Kassaby, Y. A., & Guan, W. (2020). The effect of slope aspect on vegetation attributes in a mountainous dry valley, Southwest China. *Scientific Reports*, *10*(1). https://doi.org/10.1038/s41598-020-73496-0

Yu, P., Xu, R., Abramson, M. J., Li, S., & Guo, Y. (2020). Bushfires in Australia: a serious health emergency under climate change. In *The Lancet Planetary Health* (Vol. 4, Number 1, pp. e7–e8). Elsevier B.V. https://doi.org/10.1016/S2542-5196(19)30267-0

Zahura, F. T., Bisht, G., Li, Z., McKnight, S., & Chen, X. (2024). Impact of topography and climate on post-fire vegetation recovery across different burn severity and land cover types through random forest. *Ecological Informatics*, *82*. https://doi.org/10.1016/j.ecoinf.2024.102757